



HAL
open science

Intercluster exchanges leading to hydride-centered bimetallic clusters: a multi-NMR, X-ray crystallographic, and DFT study

Yu-Jie Zhong, Jian-Hong Liao, Tzu-Hao Chiu, Ying-Yann Wu, Samia Kahlal, Michael J Mcglinchey, Jean-Yves Saillard, C W Liu

► To cite this version:

Yu-Jie Zhong, Jian-Hong Liao, Tzu-Hao Chiu, Ying-Yann Wu, Samia Kahlal, et al.. Intercluster exchanges leading to hydride-centered bimetallic clusters: a multi-NMR, X-ray crystallographic, and DFT study. Dalton Transactions, 2021, 50 (13), pp.4727-4734. 10.1039/d1dt00072a . hal-03194301

HAL Id: hal-03194301

<https://hal.science/hal-03194301>

Submitted on 23 Apr 2021

HAL is a multi-disciplinary open access archive for the deposit and dissemination of scientific research documents, whether they are published or not. The documents may come from teaching and research institutions in France or abroad, or from public or private research centers.

L'archive ouverte pluridisciplinaire **HAL**, est destinée au dépôt et à la diffusion de documents scientifiques de niveau recherche, publiés ou non, émanant des établissements d'enseignement et de recherche français ou étrangers, des laboratoires publics ou privés.

Intercluster Exchanges Leading to Hydride-Centered Bimetallic Clusters: An X-ray Crystallographic, Multi-NMR and DFT Study

Yu-Jie Zhong,^a Jian-Hong Liao,^a Tzu-Hao Chiu,^a Ying-Yann Wu,^b Samia Kahlal,^c Michael J. McGlinchey,^d Jean-Yves Saillard^c and C. W. Liu*^a

^a Department of Chemistry, National Dong Hwa University, Hualien 974301, Taiwan, Republic of China. E-mail: chenwei@mail.ndhu.edu.tw

^b Institute of Chemistry, Academia Sinica, Taipei 11528, Taiwan, Republic of China.

^c Univ Rennes, CNRS, ISCR-UMR 6226, F-35000 Rennes, France.

^d UCD School of Chemistry, University College Dublin, Belfield, Dublin 4, Ireland

Abstract

Encouraged by the successful syntheses of alloy nanoclusters (or nanoparticles) via intercluster (or interparticle) reactions, herein we apply this methodology to prepare a series of bimetallic hydride clusters. Mixing of two clusters, $[\text{Ag}_7(\text{H})\{\text{E}_2\text{P}(\text{O}^i\text{Pr})_2\}_6]$ ($\text{E} = \text{S}, 1; \text{Se}, 3$) and $[\text{Cu}_7(\text{H})\{\text{E}_2\text{P}(\text{O}^i\text{Pr})_2\}_6]$ ($\text{E} = \text{S}, 2; \text{Se}, 4$), yields two series of hydride-centered bimetallic clusters, $[\text{Cu}_x\text{Ag}_{7-x}(\text{H})\{\text{E}_2\text{P}(\text{O}^i\text{Pr})_2\}_6]$ ($x = 0 - 7; \text{E} = \text{S}, 5; \text{Se}, 6$). Their compositions are fully characterized by positive-mode ESI-MS spectrometry, multi-NMR spectroscopy, and the structures of $[\text{Cu}_6\text{Ag}(\text{H})\{\text{S}_2\text{P}(\text{O}^i\text{Pr})_2\}_6]$ (5a) and $[\text{CuAg}_6(\text{H})\{\text{Se}_2\text{P}(\text{O}^i\text{Pr})_2\}_6]$ (6a) by single crystal X-ray diffraction. The presence of individual compounds in solution is the result of a (dynamic) chemical equilibrium primarily driven by metal exchanges. In fact, the process of inter-cluster exchange of 1 and 2 leading to hydride-centered bimetallic clusters 5 can be monitored by concentration-dependent ^{31}P NMR spectroscopy of which the higher concentration of 1 in the reaction, the closer to its resonance will be the distribution, in accord with Le Chatelier's principle. The dynamic equilibrium is further confirmed by 2D exchange spectroscopy that reveals a stepwise process involving one metal exchange at a time. DFT calculations on a model series of clusters 6 show that silver prefers occupying the inner tetrahedral positions, while copper favors capping positions, in full agreement with the crystal structure of 5a and 6a.

Introduction

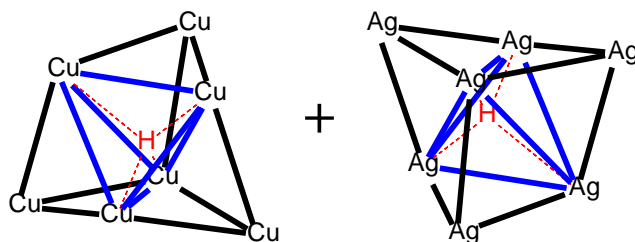
The topic of alloy nanoclusters (NCs) is currently a subject of active research, because it allows tuning (sometimes dramatically modifying) the properties of their homometallic counterparts.¹⁻⁴ Doping heterometals via galvanic/anti-galvanic exchanges or co-reductions are the most common methods to obtain heterometallic

NCs.⁵⁻⁹ Zhu and coworkers reported a library of doped Ag₂₉ NCs and successfully pushed the heterometallic boundaries to tetrametallic NCs.¹⁰ Pradeep *et al.* described the intercluster reaction of Ag₂₅(DMBT)₁₈ and Au₂₅(PET)₁₈ to produce isostructural Ag_mAu_n(SR)₁₈ species.¹¹⁻¹² Based on ESI mass spectrometry experiments, which detected a species corresponding to the [Ag₂₅Au₂₅(DMBT)₁₈(PET)₁₈]²⁻ dianion, an exchange process starting from the approach of two clusters and leading to the alloys was proposed. A possible reaction route of this intercluster alloying reaction was further theoretically studied by Pei *et al.*¹³ Successful examples produced via intercluster reactions include Au₂₂Ir₃ from Au₂₅ and Ir₉,¹⁴ Au₁₂Ag₃₂ from Au₂₅ and Ag₄₄,¹⁵ and trimetallic MAu₁₂Ag₁₆ (M = Ni, Pd, Pt) NCs from MAg₂₈ and Au₂₅.¹⁶ Intercluster reactions also occur on the surface of the NCs such as ligand replacement reactions, which are considered to trigger structural transformations under certain circumstances.¹⁷⁻¹⁹ In the present study we apply intercluster reactions as the main strategy to generate hydride-centered bimetallic clusters. It appears the latter clusters do not form through ligand exchanges but via direct metal exchanges as demonstrated by solution NMR spectroscopic studies. To the best of our knowledge, *this method has not previously been used in the synthesis of bimetallic hydride clusters.* Although polyhydrido copper clusters stabilized by chalcogenolates have received tremendous attention due to their potential applications in catalysis, electrocatalytic CO₂ reduction, hydrogenation, or energy storage,²⁰⁻²³ well-characterized bimetallic hydride clusters of group 11 metals remain scarce partly due to the lack of reliable, convenient synthetic methodologies.²⁴⁻²⁶ Importantly, the method adopted in this report is significantly different from a recent development by Tsukuda and his co-workers on the subject of hydride-mediated cluster growth involving coinage metals.²⁷⁻²⁸

Results and Discussion

We recently demonstrated that Cu₄Ag₃(H){S₂P(O^{*i*}Pr)₂}₆, in which seven metal atoms constitute a tricapped-tetrahedral framework, (μ₃-Cu)₃(CuAg₃), with an encapsulated hydride at the center of CuAg₃ tetrahedron, can be isolated from a mixture of Cu_xAg_{7-x}(H){S₂P(O^{*i*}Pr)₂}₆ (x = 1 - 6), synthesized by the reaction of [Ag(CH₃CN)₄]PF₆, [Cu(CH₃CN)₄]PF₆, NH₄[S₂P(O^{*i*}Pr)₂] and NaBH₄ in a 3:4:6:1 molar ratio.²⁴ Although both the composition and structure of a hydride-centered bimetallic heptanuclear cluster were unambiguously confirmed by X-ray diffraction, ESI-MS and NMR data from the crystalline products revealed characteristics corresponding to a distribution of hydride-centered bimetallic clusters, Cu_xAg_{7-x}(H){S₂P(O^{*i*}Pr)₂}₆ (x = 1 - 6), and suggest the occurrence of intramolecular and/or intermolecular metal exchanges both in solution and in the gas phase. Herein we present the inter-cluster reactions (Scheme 1) of [Ag₇(H){S₂P(O^{*i*}Pr)₂}₆] (1) and [Cu₇(H){S₂P(O^{*i*}Pr)₂]₆ (2), [Ag₇(H){Se₂P(O^{*i*}Pr)₂]₆ (3)

and $[\text{Cu}_7(\text{H})\{\text{Se}_2\text{P}(\text{O}^i\text{Pr})_2\}_6]$ (4), to form $[\text{Cu}_x\text{Ag}_{7-x}(\text{H})\{\text{S}_2\text{P}(\text{O}^i\text{Pr})_2\}_6]$ (5) and $[\text{Cu}_x\text{Ag}_{7-x}(\text{H})\{\text{Se}_2\text{P}(\text{O}^i\text{Pr})_2\}_6]$ (6), respectively.



Scheme 1. A schematic diagram of the $\text{Cu}_7(\text{H})$ and $\text{Ag}_7(\text{H})$ cores in two orientations. Their metal frameworks show the same tricapped tetrahedral geometry.

Characterization of the product distributions in (5) and (6) by multi-NMR spectroscopy and ESI mass spectrometry

In order to understand the exchange reaction between two different clusters, $\text{Ag}_7(\text{H})\{\text{S}_2\text{P}(\text{O}^i\text{Pr})_2\}_6$ (1) and $\text{Cu}_7(\text{H})\{\text{S}_2\text{P}(\text{O}^i\text{Pr})_2\}_6$ (2), which have unique ^{31}P resonances at 108.8 and 103.9 ppm, respectively, were synthesized as the starting materials. Time-dependent ^{31}P NMR spectra (Figure S1) in which 1 and 2 were mixed in an equimolar ratio in CDCl_3 in an NMR tube were acquired to monitor the reaction, and showed a reassembly process within one minute of mixing. A total of six resonances observed after 10 minutes are virtually identical to those of the previously published bimetallic heptametall cluster mixtures, $[\text{Cu}_x\text{Ag}_{7-x}(\text{H})\{\text{S}_2\text{P}(\text{O}^i\text{Pr})_2\}_6]$ ($x = 1 - 6$), (5).^{11a} Their chemical shifts, line shapes, and relative intensities did not change after 10 minutes, showing that the metal exchange proceeds spontaneously and reaches equilibrium in a very short time. One might therefore anticipate that a variation in the starting proportions of the reactants should influence the chemical equilibrium. To verify this hypothesis, concentration-dependent experiments were performed by mixing 1 and 2 in different ratios; 1:6, 1:4, 1:2, 1:1, 2:1, 4:1, and 6:1 (Figure 1a), and their percentage yields are listed in Table S1. Each NMR spectrum was recorded after one hour of mixing to ensure that the reaction had reached equilibrium. For example, in the case of a 1:6 molar ratio of $\text{Ag}_7:\text{Cu}_7$, the $^{31}\text{P}\{^1\text{H}\}$ NMR spectrum exhibited three resonances at 103.9, 104.3, and 104.9 ppm (Figure 1b), and the corresponding ^1H spectrum showed hydride shifts at 3.58, 5.00 and 5.51 ppm, respectively (Figure 1c). Although it is difficult to certify compositions of the corresponding compounds solely from the ^{31}P NMR spectrum, their unique ^1H -($^{107}\text{Ag}/^{109}\text{Ag}$) coupling patterns and integration ratios displayed in the ^1H NMR spectrum provide critical information to formulate compositions unambiguously.

For example, the hydride resonance centered at 5.00 ppm attributable to $\text{Cu}_6\text{Ag}(\text{H})$ appears as a pair of doublets centred at the same chemical shift. In this case, the two isotopomers, one containing ^{107}Ag , the other ^{109}Ag , each bring about doublet splitting

of the proton resonance. These two spin $\frac{1}{2}$ nuclei, which are almost equally abundant (51.82% and 48.18%, respectively), have magnetogyric ratios that differ only by a factor of 1.145, that is reflected in their J values whereby couplings to another nucleus (such as ^1H or ^{31}P) are always larger by exactly this factor in the ^{109}Ag case.

A curious feature of spectra involving coupling to silver is beautifully illustrated in the $\text{Cu}_5\text{Ag}_2(\text{H})$ system centered at 5.51 ppm. The three combinations of isotopomers, ^{107}Ag - ^{107}Ag , ^{107}Ag - ^{109}Ag and ^{109}Ag - ^{109}Ag , exist in the ratio 1:2:1 (approximately); the ^{107}Ag - ^{107}Ag and ^{109}Ag - ^{109}Ag combinations each give rise to 1:2:1 triplets with, as noted above, slightly different $J(^1\text{H}$ - $^{107}\text{Ag})$ and $J(^1\text{H}$ - $^{109}\text{Ag})$ values. Concomitantly, coupling in the ^{107}Ag - ^{109}Ag isotopomer appears as a doublet of doublets with, of course, the same $J(^1\text{H}$ - $^{107}\text{Ag})$ and $J(^1\text{H}$ - $^{109}\text{Ag})$ values seen in the aforementioned triplets. The resulting overlap of these three subspectra appears as a pseudo triplet of triplets (Figure S2), as seen in a disilver-hydride reported previously.¹² Fortunately, this simplifying pattern continues such that in the $\text{Cu}_4\text{Ag}_3(\text{H})$ and $\text{Cu}_3\text{Ag}_4(\text{H})$ clusters the overlapping sets of subspectra appear as a pseudo quartet of quartets and a pseudo quintet of quintets, respectively.

Hence, the combined analysis of both ^{31}P and ^1H NMR spectra allows unambiguous identification of the remaining compounds $\text{Cu}_x\text{Ag}_{7-x}(\text{H})\{\text{S}_2\text{P}(\text{O}^i\text{Pr})_2\}_6$, $x = 5, 6,$ and 7 . Based on this principle, all the corresponding ^{31}P NMR resonances of $\text{Cu}_x\text{Ag}_{7-x}(\text{H})\{\text{S}_2\text{P}(\text{O}^i\text{Pr})_2\}_6$, $x = 0-7$, can be reasonably assigned (Table S2, Figures S3-S8). In short, our experiments indicate that increasing the Cu content in the starting mixture results in a product distribution exhibiting a larger number of the more shielded ^{31}P resonances; in contrast, a higher concentration of the $\text{Ag}_7(\text{H})$ cluster, **1**, in the initial mixture leads to a more downfield-shifted distribution. This phenomenon is a striking illustration of Le Chatelier's principle whereby a system experiencing a disturbance (in this case, a change in concentration) responds so as to establish a new equilibrium position.

Compositions of $\text{Cu}_x\text{Ag}_{7-x}(\text{H})\{\text{S}_2\text{P}(\text{O}^i\text{Pr})_2\}_6$ ($x = 0 - 7$) were further authenticated by the positive-mode ESI mass spectrum (Figure S9). A distribution of ion peaks $[\text{Cu}_x\text{Ag}_{7-x}(\text{H})\{\text{S}_2\text{P}(\text{O}^i\text{Pr})_2\}_6 + \text{Ag}^+ + 2(\text{H}_2\text{O})]^+$, $x = 0 - 7$, was observed from which the most intense band appears at $x = 4$. Further crystalline products of $[\text{Cu}_4\text{Ag}_3(\text{H})\{\text{S}_2\text{P}(\text{O}^i\text{Pr})_2\}_6]$ were collected for mass spectrometry. Surprisingly, the ion peaks displayed a near identical distribution to that found in $\text{Cu}_x\text{Ag}_{7-x}(\text{H})\{\text{S}_2\text{P}(\text{O}^i\text{Pr})_2\}_6$, where $x = 0 - 7$. These two results strongly suggest that even though the target ion peak ($x = 4$) is observed in the mass spectrum, the other peaks are apparently generated from a reassembly process in the gas phase.

Following the same synthetic procedure, the diisopropyl diselenophosphate-protected hydride-centered bimetallic clusters, $\text{Cu}_x\text{Ag}_{7-x}(\text{H})\{\text{Se}_2\text{P}(\text{O}^i\text{Pr})_2\}_6$ ($x = 1 - 6$) (**6**), can also be obtained by the reaction of $\text{Ag}_7(\text{H})\{\text{Se}_2\text{P}(\text{O}^i\text{Pr})_2\}_6$ (**3**)¹³ and

$\text{Cu}_7(\text{H})\{\text{Se}_2\text{P}(\text{O}^i\text{Pr})_2\}_6$ (4). As with their sulfur analogues, the ^{31}P NMR spectra (Figure 2) were recorded under conditions with different initial concentrations of 3 and 4, and exhibited similar behaviour, whereby the larger the concentration of one of the reactants, the closer to its resonance was the distribution, as a result of equilibrium. However, there was also an overlapping of two of the ^{31}P resonances that could not be unequivocally resolved by cross-comparison with the corresponding ^1H spectra (Figures S10-S16) in which a hydride resonance was partially obscured by a methyl signal.

This problem was overcome by preparation of the deuteride analogues, $\text{Cu}_x\text{Ag}_{7-x}(\text{D})\{\text{Se}_2\text{P}(\text{O}^i\text{Pr})_2\}_6$, whose ^2H NMR spectra were then acquired. Since the magnetogyric ratios of ^1H and ^2H differ by a factor of 6.51, so do their corresponding $J(^1\text{H}-^{109}\text{Ag})$ and $J(^2\text{H}-^{109}\text{Ag})$ values. This decrease in the coupling to silver makes the $J(^2\text{H}-^{107}\text{Ag})$ and $J(^2\text{H}-^{109}\text{Ag})$ values too close to be differentiated, but the doublet observed at 1.22 ppm in ^2H NMR spectrum (Figure S17-S18) was found and can be assigned to the $\text{Cu}_6\text{Ag}(\text{D})\{\text{Se}_2\text{P}(\text{O}^i\text{Pr})_2\}_6$ species, thereby allowing identification of its ^{31}P signal. Chemical shift and coupling constants for these deuterium analogues are listed in Table S3.

An additional feature of series 6 is the presence of another spin $\frac{1}{2}$ nucleus, ^{77}Se , whose chemical shift also corresponds to the Ag/Cu content of the cluster. The ^1H , ^{31}P , ^{109}Ag (Figure S19), and ^{77}Se (Figure S20) chemical shifts and coupling constants of $\text{Cu}_x\text{Ag}_{7-x}(\text{H})\{\text{Se}_2\text{P}(\text{O}^i\text{Pr})_2\}_6$ ($x = 0 - 7$), and the ratio of each compound, are listed in Table 1 and Table 2, respectively.

As for 5, compositions of cluster 6 were further authenticated by ESI-MS. The crystalline sample of $\text{CuAg}_6(\text{H})\{\text{Se}_2\text{P}(\text{O}^i\text{Pr})_2\}_6$ (6a) was collected to record ESI-MS spectrometry. The positive-ion ESI mass spectrum (Figure S21) displayed the highest-intensity ion peak at m/z 2661.1 (calc. 2661.6), which can be assigned to $[\text{CuAg}_6(\text{H})\{\text{Se}_2\text{P}(\text{O}^i\text{Pr})_2\}_6 + \text{Ag}^+]^+$ (Figure S22). A distribution of $[\text{Cu}_x\text{Ag}_{7-x}(\text{H})\{\text{Se}_2\text{P}(\text{O}^i\text{Pr})_2\}_6 + \text{Ag}^+]^+$ ($x = 0-3$) observed in the spectrum indicates that the rearrangement reaction of the clusters, probably via molecular collisions, occurred in the gas phase. ESI-MS spectrum (Figure 3) of the product from the reaction of 1:1 Ag_7 , 3: Cu_7 , 4 displayed a distribution corresponding to the species $[\text{Cu}_x\text{Ag}_{7-x}(\text{H})\{\text{Se}_2\text{P}(\text{O}^i\text{Pr})_2\}_6 + \text{Ag}^+]^+$ ($x = 0-7$). The latter distribution is close to that already seen in the equimolar reaction of Ag_7 , 1, and Cu_7 , 2, to form $\text{Cu}_x\text{Ag}_{7-x}(\text{H})\{\text{Se}_2\text{P}(\text{O}^i\text{Pr})_2\}_6$.

Rationalization of the hydride-silver NMR coupling constants, $J(^1\text{H}-^{109}\text{Ag})$

As listed in Table 1, in the $\text{Ag}_7(\text{H})\{\text{Se}_2\text{P}(\text{O}^i\text{Pr})_2\}_6$ cluster, the hydride-silver coupling constant (40 ± 1 Hz) seen in both the ^1H and ^{109}Ag regimes is the average of seven interactions: $[(1 \text{ Ag}_{\text{top}} + 3 \text{ Ag}_{\text{cap}} + 3 \text{ Ag}_{\text{tri}}) \div 7]$. Of course, these are not all derived from

a single $^{109}\text{Ag}_7$ molecule that represents only a minor fraction of the $^{107}\text{Ag}_x^{109}\text{Ag}_{7-x}$ isotopomer distribution, which (for simplicity, assuming a 50/50 isotopic ratio) follows the binomial pattern 1:7:21:35:35:21:7:1. The observed $J(^1\text{H}-^{109}\text{Ag})$ values increase from 40 Hz in the $\text{Ag}_7(\text{H})$ cluster to 47 Hz, 56 Hz, and 62 Hz in the $\text{Ag}_6\text{Cu}(\text{H})$, $\text{Ag}_5\text{Cu}_2(\text{H})$ and $\text{Ag}_4\text{Cu}_3(\text{H})$ systems, respectively, and eventually reach 67 Hz and 82 Hz in the $\text{Ag}_2\text{Cu}_5(\text{H})$ and $\text{AgCu}_6(\text{H})$ clusters. It is evident that the sequential replacement by Cu of capping sites previously occupied by ^{109}Ag brings about a marked increase in the average $^1\text{H}-^{109}\text{Ag}$ coupling constant. These data are entirely consistent with the major contributors to the coupling being the $^1J(^1\text{H}-^{109}\text{Ag})$ interactions with the four directly bonded "tetrahedral" silvers, and that any $^2J(^1\text{H}-^{109}\text{Ag})$ interactions with the face-capping atoms are zero (or at least very small). Finally, we note that in the analogous sulfur complexes, 5, the pattern of J values (Table S2) is very similar, but all are slightly larger.²⁴

Dynamic equilibrium and intercluster exchanges studied by NMR spectroscopy

In an experiment starting with equimolar quantities of $\text{Ag}_7(\text{H})\{\text{S}_2\text{P}(\text{O}^i\text{Pr})_2\}_6$, 1, and $\text{Cu}_7(\text{H})\{\text{S}_2\text{P}(\text{O}^i\text{Pr})_2\}_6$, 2, which yields the largest number of products, *i.e.*, $\text{Cu}_x\text{Ag}_{7-x}(\text{H})\{\text{S}_2\text{P}(\text{O}^i\text{Pr})_2\}_6$ ($x = 0 - 6$), a number of $^{31}\text{P}-^{31}\text{P}\{^1\text{H}\}$ 2D EXSY (exchange spectroscopy) NMR spectra were recorded. In such experiments, the observation of off-diagonal peaks reveals which species are undergoing exchange. A spectrum acquired at ambient temperature with a mixing time of 400 ms appears as Figure 4a, in which cross peaks appear, for example, between Ag_7H and CuAg_6H , CuAg_6H and $\text{Cu}_2\text{Ag}_5\text{H}$, $\text{Cu}_2\text{Ag}_5\text{H}$ and $\text{Cu}_3\text{Ag}_4\text{H}$, but none between peaks assignable to Ag_7H and $\text{Cu}_2\text{Ag}_5\text{H}$, or to $\text{Cu}_2\text{Ag}_5\text{H}$ and $\text{Cu}_4\text{Ag}_3\text{H}$. Evidently, on this time scale (400 ms), exchange only takes place between systems that differ in content by only a single silver, and not between species more widely separated. However, as the mixing time increases to 800 ms (Figure 4b), the appearance of additional (but less intense) cross peaks illustrates that each cluster can be further exchanged, as in $\text{Ag}_7\text{H} \rightleftharpoons \text{Cu}_2\text{Ag}_5\text{H}$; $\text{CuAg}_6\text{H} \rightleftharpoons \text{Cu}_3\text{Ag}_4\text{H}$; $\text{Cu}_2\text{Ag}_5\text{H} \rightleftharpoons \text{Cu}_4\text{Ag}_3\text{H}$, etc., in each case a difference of two coppers and two silvers. These results unequivocally suggest the operation of a stepwise process, exchanging one metal at a time via $\text{Ag}_7\text{H} \rightleftharpoons \text{CuAg}_6\text{H} \rightleftharpoons \text{Cu}_2\text{Ag}_5\text{H}$, etc. and *vice versa*.

As to the question of which atom is exchanging, we strongly favor the idea of exchanges occurring at metal centers over that of ligand exchanges; both $d^{10}-d^{10}$ and H-Ag interactions are weaker than S-Ag covalent bonding, therefore the metals are more labile than the templating ligands. As a result, the metal exchange process starts from both ends (Cu_7 and Ag_7), gradually approaching the middle, and eventually spontaneously achieves equilibrium. The central limit theorem (CLT) states that the distribution of resonances approximate a normal distribution (bell distribution).¹⁴ Thus

the highest intensity of the NMR peaks will fall near the middle of the spectrum, in this case $\text{Cu}_4\text{Ag}_3(\text{H})\{\text{S}_2\text{P}(\text{O}^i\text{Pr})_2\}_6$.

One can discount the existence of ligand exchange in the above-mentioned reactions since this would lead to random exchange between all species, in disagreement with the observed EXSY data. Thus, the $\text{Cu}_x\text{Ag}_{7-x}(\text{H})\{\text{S}_2\text{P}(\text{O}^i\text{Pr})_2\}_6$ ($x = 1 - 6$) species are formed through inter-cluster metal exchange processes, and is obviously different from the thio-protected nanoclusters formed through ligand exchanges in the inter-cluster reaction.^{4,5,15}

Likewise, the ^1H - ^1H 2D EXSY NMR spectrum, recorded with a mixing time of 400 ms (Figure S23), only showed cross peaks between adjacent clusters, such as Cu_6AgH and $\text{Cu}_5\text{Ag}_2\text{H}$, in complete accord with the corresponding ^{31}P - $^{31}\text{P}\{^1\text{H}\}$ 2D EXSY data. Clearly, the individual compounds $\text{Cu}_x\text{Ag}_{7-x}(\text{H})\{\text{S}_2\text{P}(\text{O}^i\text{Pr})_2\}_6$ ($x = 0 - 6$) are not static in solution, but are undergoing (dynamic) intermolecular exchange.

We note also that, as shown in Figure S23, cross-peaks within each individual cluster are evident, revealing an intramolecular exchange at least as rapid as the intermolecular process. This is supported by the observation that even at -60°C no changes to the hydride splitting pattern become apparent.^{11a} Furthermore, as noted above, within each component of the rapidly equilibrating set of clusters, there is only a single ^{109}Ag , ^{31}P or ^{77}Se resonance, once again supporting the assertion of rapid intramolecular metal scrambling that also brings about averaging of the different $J(^1\text{H}$ - $^{109}\text{Ag})$ values.

These data, together with the observation of a single ^{31}P resonance in each of the starting Ag_7 or Cu_7 clusters, 1 – 4, and the pseudo octet of octets character of the hydride in 1, are all consistent with the dynamic nature of the hydride-centered tricapped tetrahedral metal core ($\text{H}@M_4@M_3$) of C_3 symmetry, whether it is homo-metallic or hetero-metallic.^{11a,13,16} One can speculate as to the mechanism of this fluxional behaviour, and a process involving rapid interchange of the seven metal vertices over eight sites (the central tetrahedron and its four capping positions),¹⁷ may be a viable option. After mixing, and achieving equilibrium, the product ratios do not change as long as the system remains undisturbed; on the other hand, each compound at the equilibrium state is still undergoing rapid metal exchange within the S_{12} (Se_{12}) icosahedral cage formed by six dichalcogenolate ligands.¹⁶⁻¹⁸ One might also tentatively suggest a mechanism for the inter-cluster exchange process whereby only a single silver or copper is replaced in the first step. If two clusters collide and there is transfer of a single metal unit onto the vacant fourth cap of the recipient cluster, with subsequent transfer back of a different metal moiety, this may account for the experimental observations.

In principle, since the inter-cluster exchange can be observed on the millisecond scale from the EXSY 2D NMR spectra, an equilibrium constant (Scheme S2) associated with

intercluster reactions (Scheme S1) might be established. Theoretically it could be verified by substituting the concentration of each compound into the equation developed. The concentrations derived from the percentage yield (Table S1) can be roughly estimated from the integration of the ^{31}P NMR spectrum; unfortunately, however, only seven species can be detected in the NMR spectrum of the 1:1 (Cu_7):(Ag_7) reaction, thus rendering this approach no longer viable.

Crystallographic studies and theoretical calculations of hydride-centered heptanuclear clusters

Upon crystallizing the products from the reaction having an initial 1:6 molar ratio of Ag_7 , 1: Cu_7 , 2, one might have expected that the major product to be $\text{Cu}_6\text{Ag}(\text{H})\{\text{S}_2\text{P}(\text{O}^i\text{Pr})_2\}_6$ because of its relatively high intensity in the ^{31}P NMR spectrum. Surprisingly, however, the X-ray structure of 5a revealed a co-crystallization product consisting of $[\text{Cu}_6\text{Ag}(\text{H})\{\text{S}_2\text{P}(\text{O}^i\text{Pr})_2\}_6]$ and $[\text{Cu}_7(\text{H})\{\text{S}_2\text{P}(\text{O}^i\text{Pr})_2\}_6]$ in a 2:1 ratio. The phenomenon of co-crystallization in which either different atoms occupy the same site of the lattice, or compositionally distinct clusters co-exist in the lattice, is becoming more common in the atomically precise nanocluster domain.¹⁹ The cluster $\text{CuAg}_6(\text{H})\{\text{Se}_2\text{P}(\text{O}^i\text{Pr})_2\}_6$, 6a, was crystallized from the reaction of Ag_7 , 3, and Cu_7 , 4, in a 6:1 molar ratio. The metal framework of structures 2, 5a, and $\text{Cu}_4\text{Ag}_3(\text{H})\{\text{S}_2\text{P}(\text{O}^i\text{Pr})_2\}_6$,^{11a} and 6a reveals the same tricapped tetrahedral cage (Figure 5a, S31-S33) encapsulating a hydride in its center. Three structures were further stabilized by dithio-(diseleno-)phosphate ligands (Figure 5b). The Ag atom in 5a is disordered at three M_{tri} and one M_{top} positions of a tricapped tetrahedral M_7 cage, $(\text{Cu}_3)_{\text{cap}}(\text{AgCu}_3)_{\text{Td}}$ (Figure S32), and the Cu atom in 6a is disordered at three M_{cap} positions to form a $(\text{CuAg}_2)_{\text{cap}}(\text{Ag}_4)_{\text{Td}}$ cage (Figure S33). Distances of $M_{\text{tri}}\text{-}M_{\text{tri}}$ and $M_{\text{top}}\text{-}M_{\text{tri}}$ in 2 are 2.8189(15)-2.8979(17) Å (avg. 2.8617(16) Å) and 2.9266(13)-2.6520(13) Å (avg. 2.9539(13) Å), which are smaller than the distances in 5a (2.782(2)-3.113(3) Å, avg. 2.906(2) Å; 3.055(2)-3.112(2) Å, avg. 3.085 Å), $\text{Cu}_4\text{Ag}_3(\text{H})\{\text{S}_2\text{P}(\text{O}^i\text{Pr})_2\}_6$ ^{11a} (2.9938(4)-3.0148(4) Å, avg. 3.0035(4) Å; 3.0970(5)-3.2543(5) Å, avg. 3.1697 Å), and 6a (2.1468(10)-2.1811(9) Å, avg. 3.1608(10) Å; 3.0584(8)-3.1396(10) Å, avg. 3.1090(9) Å). The largest tetrahedron is in 6a and the smallest one is in 2, and can be attributed to the number of Ag atoms that locate on the tetrahedron: $(\text{Cu}_4)_{\text{Td}}$ in 2, $(\text{AgCu}_3)_{\text{Td}}$ in 5a, $(\text{Ag}_3\text{Cu})_{\text{Td}}$ in Cu_4Ag_3 ,^{11a} and $(\text{Ag}_4)_{\text{Td}}$ in 6a. The relative order of bond lengths has the same trend in other distances such as $M_{\text{cap}}\text{-}M_{\text{top}}$ and $M_{\text{cap}}\text{-}M_{\text{tri}}$. The selected bond lengths in structures 2, 5a, $\text{Cu}_4\text{Ag}_3(\text{H})\{\text{S}_2\text{P}(\text{O}^i\text{Pr})_2\}_6$, and 6a are listed in Table 3. In general, silver atoms located in the tetrahedral positions in 5a have lower energy than those in capping positions, whereas copper atoms located in capping positions have lower energy than in

tetrahedral positions. This trend echoes the situation in our previously published sulfur analogues.^{11a}

DFT calculations at the BP86-D3/ Def2-TZVP level (see Computational details) were performed on simplified models of clusters 3, 4 and 6, namely 3', 4' and 6', in which the isopropoxy groups were replaced by hydrogens. In the case of the heterometallic 6' series, all the positional isomers for each individual composition were considered. Their core topology and energetic data are reported in Figure S34, together with the associated ¹H NMR computed chemical shift. The metal cores of the lowest energy isomers within the 6' series are shown in Figure 6. The homometallic species 3' and 4' exhibit a structure of ideal C₃ symmetry, with a rather regular inner tetrahedron. The H-M_{tri} and H-M_{top} distances are respectively 1.707 and 1.713 Å (3') and 1.946 and 1.871 Å (4'). The optimized structures of the bimetallic clusters 6' tend to retain as much as possible this structural feature, although some of them are substantially distorted. From the relative energies of the various positional isomers, one can see that the general site preference for Ag is M_{tri} > M_{top} > M_{cap}. The situation is more or less reversed for Cu with M_{cap} ≈ M_{top} > M_{tri}. It is of note that calculations performed at the same level of theory on the sulfur analogues of 3', 4' and 6' provided similar results.^{11a} These results are in line with the X-ray structures of 5a and 6a, as found previously for their Cu₃Ag₄ and Cu₄Ag₃ dithiophosphate analogues.^{11a} On the other hand, the ¹H NMR chemical shifts (Figure Sa) computed for the lowest isomers of the Cu_xAg_{7-x} series do not all fit with the recorded experimental values (Table 1). The former show strong dependence on the number of Cu atoms on the inner tetrahedron, whereas the latter varies with x, *i.e.* the total number of Cu atoms in the cluster. This observation can be interpreted on the basis of fast intramolecular exchange between several isomers in solution on the NMR time scale. This is consistent with the fact that each cluster exhibits only a single ¹H, ¹⁰⁹Ag and ²¹P resonance (see above).

Conclusion

In conclusion, hydride-centered bimetallic clusters can be conveniently synthesized by simply mixing two hydride-centered homoleptic, homometallic clusters, Ag₇(H)(dtp/dsep)₆ and Cu₇(H)(dtp/dsep)₆, which are covered by six dichalcogenophosphates. The reaction is spontaneous and fast, resulting in a mixture of Cu_xAg_{7-x}(H){E₂P(O^{*i*}Pr)₂}₆ (x = 0-7; E = S, Se) within 10 minutes. The tendency to reach equilibrium in solution is driven by a stepwise, one-metal exchange process, as revealed by 2D EXSY NMR experiments. The concentration-dependent experiment confirmed that this chemical equilibrium can be disturbed by changing the stoichiometric ratio of reactants in accord with Le Chatelier's principle. We trust that intercluster reactions leading to the formation of hydride-centered bimetallic clusters

presented here may provide a new synthetic avenue towards the future discovery of more closed-shell, anion-centered bimetallic or even multimetallic clusters.

In closing, we wonder whether the products identified in the ESI-MS spectra of $\{[Ag_mAu_n(SR)_{18}]^-, m + n = 25\}^{11-12}$ derived from interparticle reactions also display dynamic equilibrium in solution, analogous to the behavior of the $Cu_xAg_{7-x}(H)\{S_2P(O^iPr)_2\}_6$ ($x = 1-6$) system discussed here. Clearly, this merits further investigation and, if true, would provide another important advance in the chemistry of nanomaterials

Conflicts of interest

The authors declare no competing financial interest.

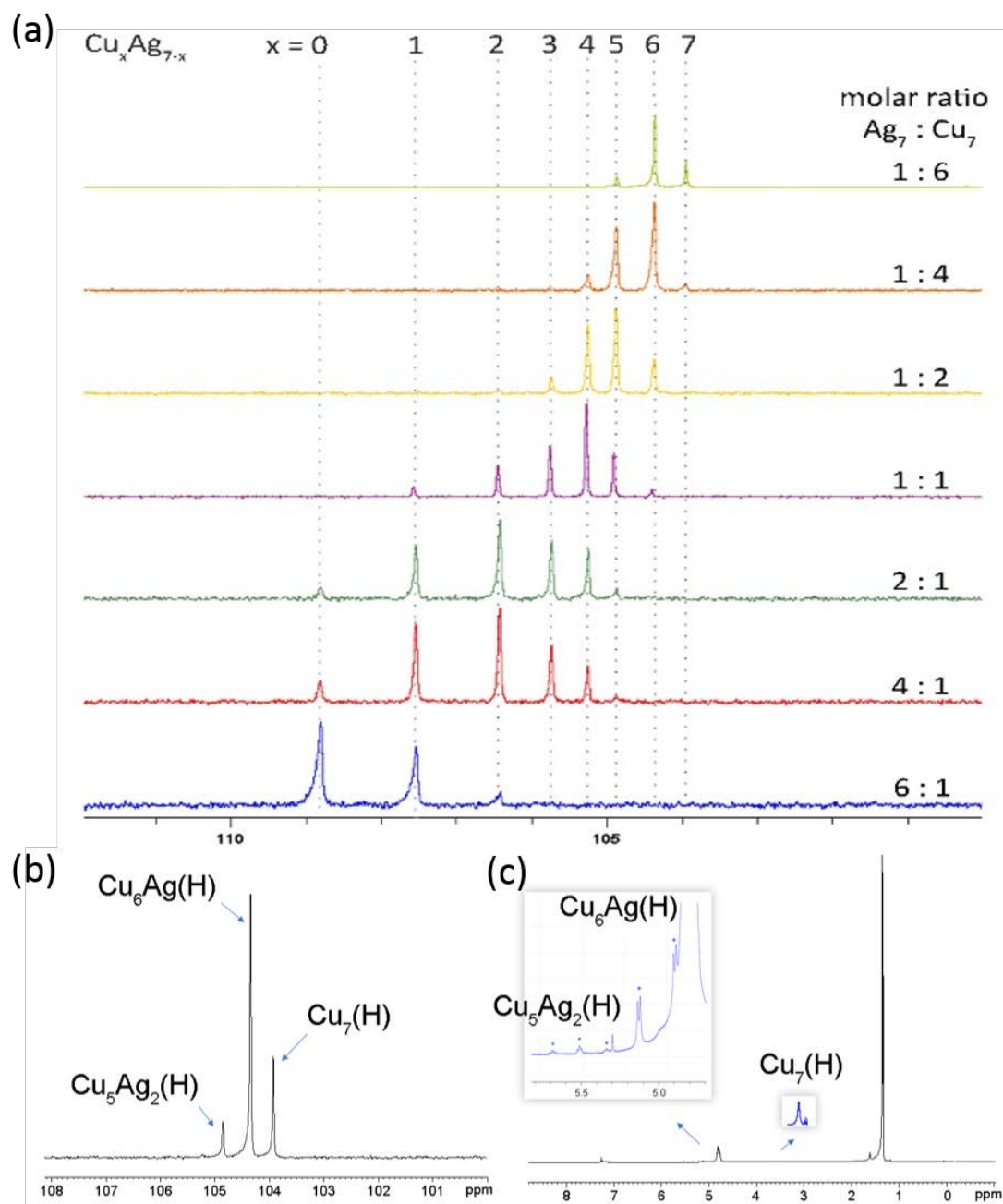
Acknowledgements

This work was supported by the Ministry of Science and Technology of Taiwan (MOST 109-2113-M-259-008, 108-2923-M-259-001), and the France-Taiwan ANR-MOST program (project Nanoalloys). We thank Academia Sinica High-Field NMR Center (HFNMRC) for technical support; HFNMRC is funded by Academia Sinica Core Facility and Innovative Instrument Project (AS-CFII-108-112). The GENCI (Grand Equipment National de Calcul Intensif) is acknowledged for HPC resources (Project A0050807367).

References

1. X. Kang, Y. Li, M. Zhu and R. Jin, *Chem. Soc. Rev.*, 2020, **49**, 6443-6514.
2. X. Kang and M. Zhu, *Chem. Soc. Rev.*, 2019, **48**, 2422-2457.
3. Q. Li, J. Chai, S. Yang, Y. Song, T. Chen, C. Chen, H. Zhang, H. Yu and M. Zhu, *Small*, in press, DOI: 10.1002/smll.201907114.
4. K. Kwak and D. Lee, *Acc. Chem. Res.*, 2019, **52**, 12-22.
5. X. Zhou, Y. Li, X. Kang, X. Wei, S. Wang, X. Meng and M. Zhu, *J. Phys. Chem. Lett.*, 2020, **11**, 2272-2276.
6. L. Liao, S. Zhou, Y. Dai, L. Liu, C. Yao, C. Fu, J. Yang and Z. Wu, *J. Am. Chem. Soc.*, 2015, **137**, 9511-9514.
7. S. Sharma, K. K. Chakrahari, J.-Y. Saillard and C. W. Liu, *Acc. Chem. Res.*, 2018, **24**, 14352-14357.
8. W.-T. Chang, P.-Y. Lee, J.-H. Liao, K. K. Chakrahari, S. Kahlal, Y.-C. Liu, M.-H. Chiang, J.-Y. Saillard and C. W. Liu, *Angew. Chem. Int. Ed.*, 2017, **56**, 10178-10182.
9. W.-T. Chang, S. Sharma, J.-H. Liao, S. Kahlal, Y.-C. Liu, M.-H. Chiang, J.-Y. Saillard and C. W. Liu, *Chem. Eur. J.*, 2018, **24**, 14352-14357.
10. X. Kang, X. Wei, S. Jin, Q. Yuan, X. Luan, Y. Pei, S. Wang, M. Zhu and R. Jin, *PNAS*, 2019, **116**, 18834-18840.
11. K. R. Krishnadas, A. Bakshi, A. Ghosh, G. Natarajan and T. Pradeep, *Nat. Commun.*, 2016, **7**, 13447.
12. K. R. Krishnadas, A. Bakshi, A. Ghosh, G. Natarajan, A. Som and T. Pradeep, *Acc. Chem. Res.*, 2017, **50**, 1988-1996.

13. B. Huang and Y. Pei, *J. Mater. Chem. A*, 2020, **8**, 10242-10251.
14. S. Bhat, A. Baksi, S. K. Mudedla, G. Natarajan, V. Subramanian and T. Pradeep, *J. Phys. Chem. Lett.*, 2017, **8**, 2787-2793.
15. K. R. Krishnadas, A. Baksi, A. Ghosh, G. Natarajan and T. Pradeep, *ACS Nano*, 2017, **11**, 6015-6023.
16. E. Khatun, P. Chakraborty, B. R. Jacob, G. Paramasivam, M. Bodiuzzaman, W. A. Dar and T. Pradeep, *Chem. Mater.*, 2020, **32**, 611-619.
17. X. Kang and M. Zhu, *Chem. Mater.*, 2019, **31**, 9939-9969.
18. X. Kang, L. Huang, W. Liu, L. Xiong, Y. Pei, Z. Sun, S. Wang, S. Wei and M. Zhu, *Chem. Sci.*, 2019, **10**, 8685-8693.
19. Q. Yao, V. Fung, C. Sun, S. Huang, T. Chen, D.-e. Jiang, J. Y. Lee and J. Xie, *Nat. Commun.*, 2018, **9**, 1979.
20. R. Poli and M. Peruzzini, *Recent Advances in Hydride Chemistry* 1st Edition. Elsevier: Amsterdam, 2001, p 557.
21. Q. Tang, Y. Lee, W. Choi, D. Lee and D.-e. Jiang, *J. Am. Chem. Soc.*, 2017, **139**, 9728-9736.
22. R. S. Dhayal, W. E. van Zyl and C. W. Liu, *Acc. Chem. Res.*, 2016, **49**, 86-95.
23. X. Du and R. Jin, *ACS Nano*, 2019, **13**, 7383-7387.
24. Y.-J. Zhong, J.-H. Liao, T.-H. Chiu, Y.-Y. Wu, S. Kahlal, J.-Y. Saillard and C. W. Liu, *Chem. Commun.*, 2020, **56**, 9300-9303.
25. A. N. Desnoyer, A. Nicolay, M. S. Ziegler, N. A. Torquato and T. D. Tilley, *Angew. Chem. Int. Ed.*, 2020, **59**, 12769-12773.
26. C. Sun, B. K. Teo, C. Deng, J. Lin, G.-G. Luo, C.-H. Tung and D. Sun, *Coord. Chem. Rev.*, 2021, **427**, 213576.
27. S. Takano, H. Hirai, S. Muramatsu and T. Tsukuda, *J. Am. Chem. Soc.*, 2018, **140**, 12314-12317.
28. H. Hirai, S. Takano and T. Tsukuda, *ACS Omega*, 2019, **4**, 7070-7075.
29. B. K. Tate, C. M. Wyss, J. Bacsá, K. A. Kluge, L. Gelbaum and J. P. Sadighi, *Chem. Sci.*, 2013, **4**, 3068-3074.
30. C. W. Liu, Y.-R. Lin, C.-S. Fang, C. Latouche, S. Kahlal and J.-Y. Saillard, *Inorg. Chem.*, 2013, **52**, 2070-2077.
31. A. Lyon, *Brit. J. Philos. Sci.*, 2013, **65**, 621-649.
32. N. Yan, N. Xia and Z. Wu, *Small*, 2020, 2000609.
33. C. A. Hosier, I. D. Anderson and C. J. Ackerson, *Nanoscale*, 2020, **12**, 6239-6242.
34. G. Salassa, A. Sels, F. Mancin and T. Bürgi, *ACS Nano*, 2017, **11**, 12609-12614.
35. C. Latouche, S. Kahlal, Y.-R. Lin, J.-H. Liao, E. Furet, C. W. Liu and J.-Y. Saillard, *Inorg. Chem.*, 2013, **52**, 13253-13262.
36. C. W. Liu, H.-W. Chang, C.-S. Fang, B. Sarkar and J.-Y. Wang, *Chem. Commun.*, 2010, **46**, 4571-4573.
37. C. W. Liu, H.-W. Chang, B. Sarkar, J.-Y. Saillard, S. Kahlal and Y.-Y. Wu, *Inorg. Chem.*, 2010, **49**, 468-475.
38. P.-K. Liao, K.-G. Liu, C.-S. Fang, C. W. Liu, J. P. Fackler Jr. and Y.-Y. Wu, *Inorg. Chem.*, 2011, **50**, 8410-8417.
39. J.-H. Liao, H.-W. Chang, Y.-J. Li, C.-S. Fang, B. Sarkar, W. E. van Zyl and C. W. Liu, Anion templating from a silver(I) dithiophosphate 1D polymer forming discrete cationic and neutral octa- and decanuclear silver(I) clusters. *Dalton Trans.*, 2014, **43**, 12380-12389.
40. P.-K. Liao, C.-S. Fang, Y.-Y. Wu and C. W. Liu, *J. Clust. Sci.*, 2019, **30**, 1185-1193.
41. X. Kang and M. Zhu, *ACS Materials Lett.*, 2020, **2**, 1303-1314.



M. Bodiuzzaman, W. A. Dar and T. Pradeep, *Small*, 2020, 2003981 **Figure 1.** (a) Concentration-dependent $^{31}\text{P}\{^1\text{H}\}$ NMR spectra (121.49 MHz) were performed by mixing **1** and **2** with stoichiometric ratios of 1:6, 1:4, 1:2, 1:1, 2:1, 4:1, and 6:1, respectively. (b) $^{31}\text{P}\{^1\text{H}\}$ and (c) ^1H NMR spectra from the reaction of $\text{Ag}_7(\text{H})\{\text{S}_2\text{P}(\text{O}^i\text{Pr})_2\}_6$ (**1**) and $\text{Cu}_7(\text{H})\{\text{S}_2\text{P}(\text{O}^i\text{Pr})_2\}_6$ (**2**) in a 1:6 molar ratio.

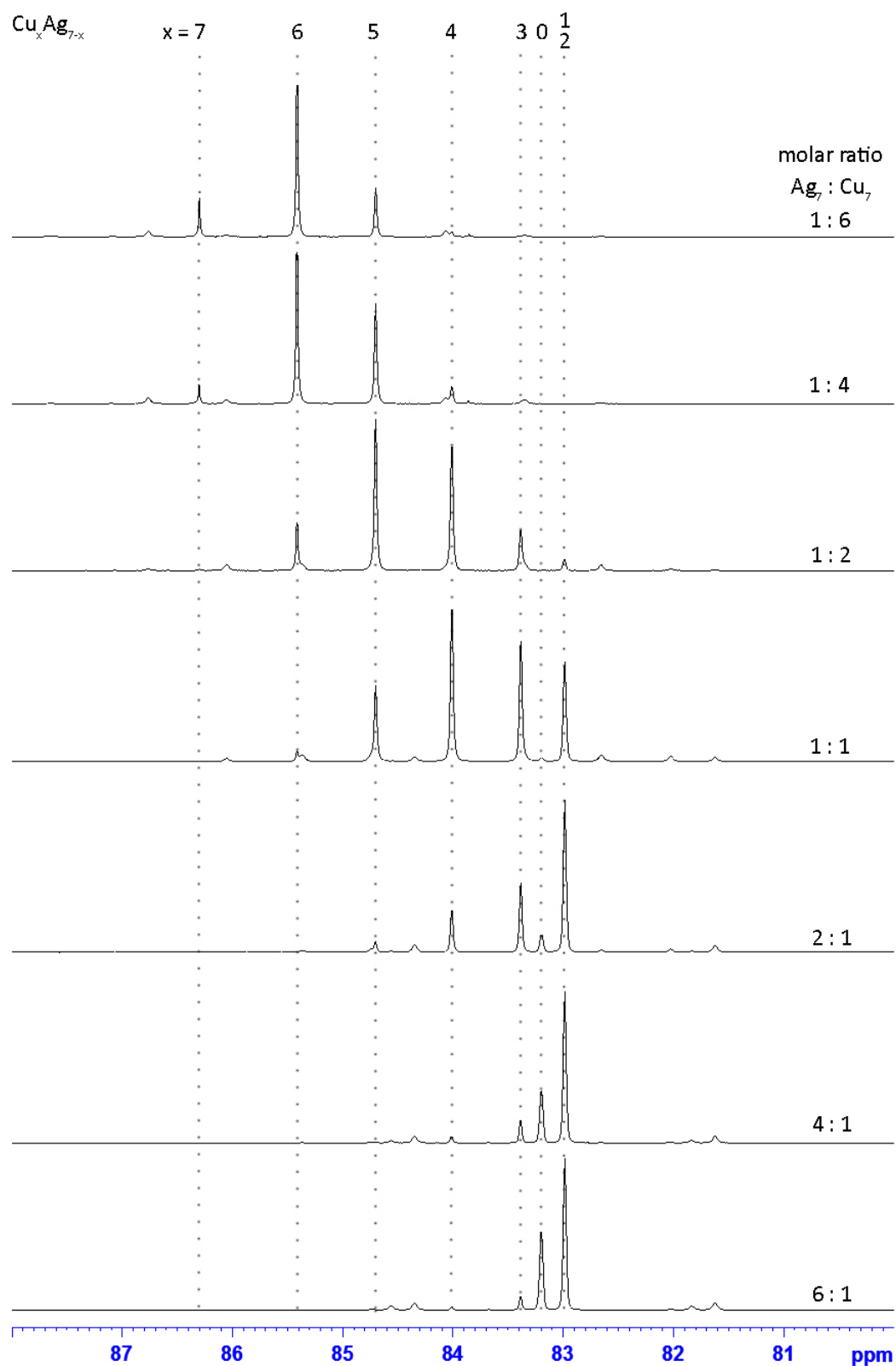


Figure 2. Concentration-dependent $^{31}\text{P}\{^1\text{H}\}$ NMR (242.86 MHz) spectra were performed by mixing **3** and **4** with stoichiometric ratios of 1:6, 1:4, 1:2, 1:1, 2:1, 4:1, and 6:1, respectively.

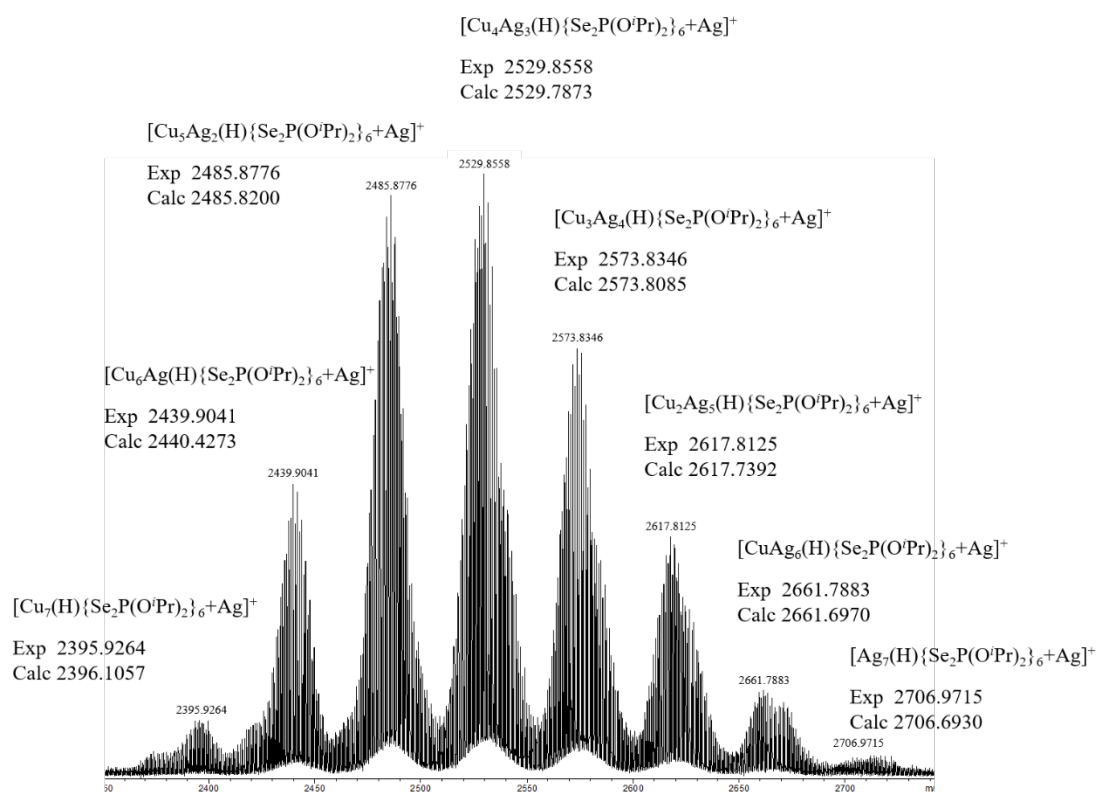


Figure 3. The positive-mode ESI mass spectrum from the reaction of $\text{Ag}_7(\text{H})\{\text{Se}_2\text{P}(\text{O}^i\text{Pr})_2\}_6$ (**3**) and $\text{Cu}_7(\text{H})\{\text{Se}_2\text{P}(\text{O}^i\text{Pr})_2\}_6$ (**4**) in a 1:1 molar ratio.

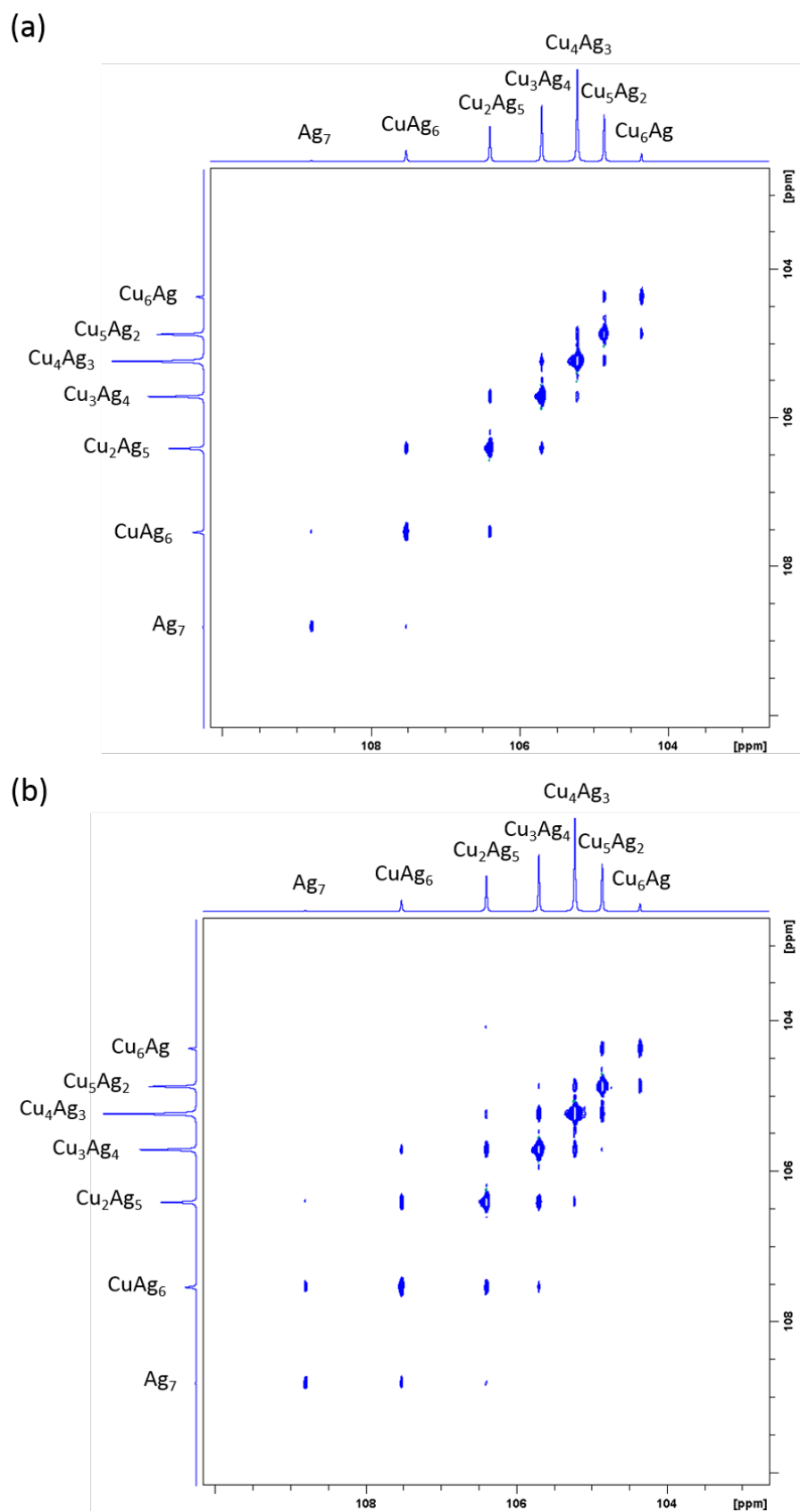


Figure 4. ^{31}P - $^{31}\text{P}\{^1\text{H}\}$ 2D EXSY NMR spectrum of the resulting $\text{Cu}_x\text{Ag}_{7-x}(\text{H})\{\text{S}_2\text{P}(\text{O}^i\text{Pr})_2\}_6$ ($x = 0 - 6$) products from the reaction of **1** and **2** at an equal molar ratio (a) recorded with a mixing time of 400 ms, and (b) 800 ms.

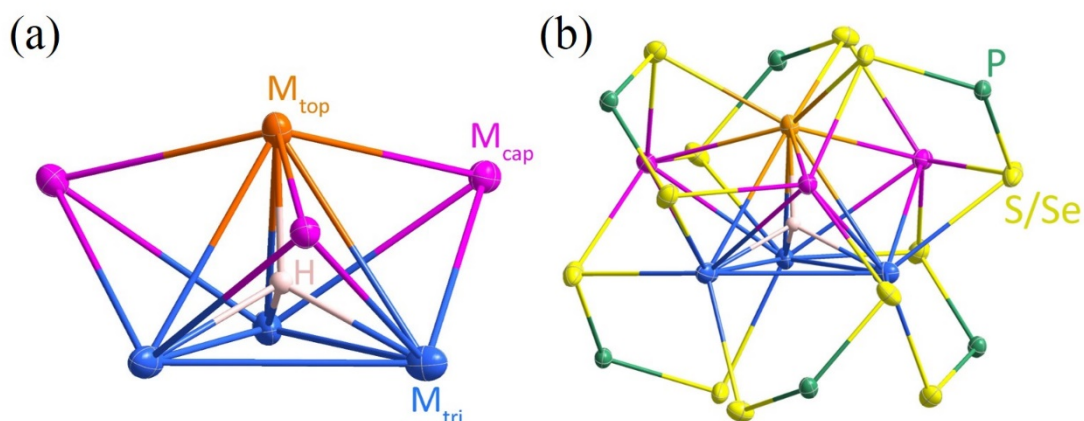


Figure 5. (a) The M_7 framework displayed a tricapped tetrahedral cage encapsulated one hydride atom in its center. (b) The M_7H core is protected by six dithio(diseleno)-phosphate ligands with isopropoxy groups omitted for clarity.

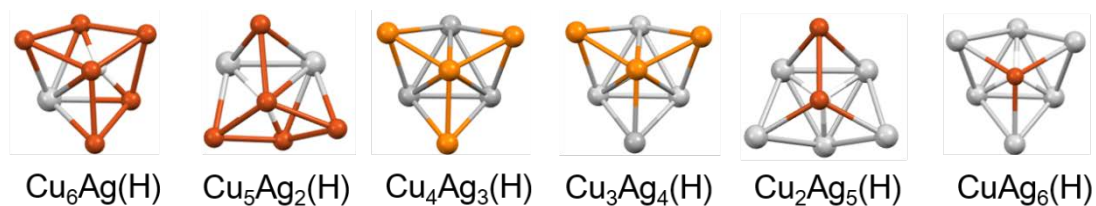


Figure 6. The metal cores of the computed lowest energy isomers within the $6'$ series.

Table 1. The chemical shifts and coupling constants of $\text{Cu}_x\text{Ag}_{7-x}(\text{H})\{\text{Se}_2\text{P}(\text{O}^i\text{Pr})_2\}_6$ (**6**).

	^1H			^{109}Ag DEPT		$^{31}\text{P}\{^1\text{H}\}$		^{77}Se	
	Chemical shift	$^1J_{\text{H-}^{107}\text{Ag}}$ (Hz)	$^1J_{\text{H-}^{109}\text{Ag}}$ (Hz)	Chemical shift	$^1J_{\text{H-}^{109}\text{Ag}}$ (Hz)	Chemical shift	$^1J_{\text{P-}^{77}\text{Se}}$ (Hz)	Chemical shift	$^1J_{\text{P-}^{77}\text{Se}}$ (Hz)
Cu₇	-0.286	-	-	-	-	86.3	653.6	25.3	659.1
Cu₆Ag₁	1.203	69.8	80.2	1036.7	83.1	85.4	655.8	24.3	656.8
Cu₅Ag₂	1.890	58.3	67.0	1096.8	67.1	84.7	656.5	26.2	671.6
Cu₄Ag₃	2.567	57.6	66.2	1138.7	67.6	84.0	658.8	26.8	647.6
Cu₃Ag₄	2.881	53.8	61.9	1158.7	62.4	83.4	660.2	28.7	660.2
Cu₂Ag₅	3.175	49.2	56.6	1154.8	56.1	83.0	661.3	28.4	659.1
Cu₁Ag₆	3.391	42.4	48.7	1137.5	45.9	83.0	661.3	28.4	659.1
Ag₇	3.557	36.0	41.4	1123.1	39.1	83.2	662.2	27.4	660.2

Table 2. Ratios of each compound in **6**. The percentage yield is calculated based on the integration of each peak in ^{31}P NMR spectra.

Cu₇:Ag₇	6 : 1	4 : 1	2 : 1	1 : 1	1 : 2	1 : 4	1 : 6
ratio	^{31}P (%)						
Cu₇	12.1	5.0	0.3				
Cu₆Ag₁	63.7	51.5	11.2	1.5	0.1		
Cu₅Ag₂	22.2	36.9	39.6	15.6	3.2	0.3	
Cu₄Ag₃	1.9	6.6	35.3	34.3	14.0	2.6	1.1
Cu₃Ag₄			10.4	25.5	22.2	8.7	5.1
Cu₂Ag₅ + Cu₁Ag₆			3.2	23.1	53.2	64.1	59.9
Ag₇					7.2	24.4	33.9

Table 3. Selected bond lengths in structures **2**, **5a**, $\text{Cu}_4\text{Ag}_3(\text{H})\{\text{S}_2\text{P}(\text{O}^i\text{Pr})_2\}_6$, ^{11a} and **6a**.

	$\text{Cu}_7(\text{H})\{\text{S}_2\text{P}(\text{O}^i\text{Pr})_2\}_6$ (2)	$\text{Cu}_6\text{Ag}(\text{H})\{\text{S}_2\text{P}(\text{O}^i\text{Pr})_2\}_6$ in 5a	$\text{Cu}_4\text{Ag}_3(\text{H})\{\text{S}_2\text{P}(\text{O}^i\text{Pr})_2\}_6$	$\text{CuAg}_6(\text{H})\{\text{Se}_2\text{P}(\text{O}^i\text{Pr})_2\}_6$ (6a)
M_{tri}-M_{tri} (Å)	2.8189(15)-2.8979(17), 2.8617(16) avg.	2.782(2)-3.113(3), 2.906(2) avg.	2.9938(4)-3.0148(4), 3.0035(4) avg.	3.1468(10)-3.1811(9), 3.1608(10) avg.
M_{top}-M_{tri} (Å)	2.9266(13)-2.9793(14), 2.9539(13) avg.	3.055(2)-3.112(2), 3.085(2) avg.	3.0970(5)-3.2543(5), 3.1697 avg.	3.0584(8)-3.1396(10), 3.1090(9) avg.
M_{cap}-M_{top} (Å)	2.6116(13)-2.6520(13), 2.6286(13) avg.	2.665(2)-2.772(2), 2.718(2) avg.	2.7152(6)-2.7312(6), 2.7235(6) avg.	2.8986(10)-2.9201(10), 2.9071(10) avg.
M_{cap}-M_{tri} (Å)	2.6990(13)- 2.7757(13), 2.7315(13) avg.	2.712(2)-2.853(2), 2.785(2) avg.	2.8950(5)- 3.0118(6), 2.9418(5) avg.	2.9993(10)-3.0726(10), 3.031(1) avg.
H-M_{top} (Å)	1.7034(8)	1.76(10)	1.65(2)	1.7387(6)
H-M_{tri} (Å)	1.7678(11)-1.8821(13), 1.8128(12) avg.	1.63(10)-2.06(10), 1.88(10) avg.	1.96(3) -2.02(3), 2.00(3) avg.	1.9803(7)-1.9918(8), 1.9844(8) avg.

Table of contents

